Effect of stacking fault energy on irradiation damage in reduced activation high entropy alloys

N. Hashimoto[1]*, E. Wada[2], H. Oka[1]

[1]*Faculty of Engineering*, *Hokkaido University, Sapporo, 060-8628 Japan*
[2]*Graduate School of Engineering*, *Hokkaido University, Sapporo, 060-8628 Japan*

Abstract

In order to investigate the effect of stacking fault energy on microstructural evolution in reduced activation high entropy alloys, electron and/or Au^+ ion irradiation was performed to the Co-free FCC-type $FeCr_{0.8}Ni_xMn_y$ (x, y = 1, 1.3, 1.5) alloys. TEM observation of the 5%-deformed $FeCr_{0.8}Ni_xMn_y$ alloys revealed the increase in the stacking fault energy with increasing both Ni and Mn concentration. In addition, $FeCr_{0.8}Ni_{1.5}Mn_{1.5}$ had the highest stacking fault energy, which was much higher value than that of 316SS. Furthermore, the yield strength and the elongation of deformed $FeCr_{0.8}Ni_xMn_y$ also showed the Ni and Mn concentration dependence. The electron irradiation at 400 ºC resulted in the formation of black dots, self-interstitial atom faulted loops, but no observable voids in all the $FeCr_{0.8}Ni_xMn_y$ alloys. The comparison of microstructural evolution revealed less faulted loop formation and growth in $FeCr_{0.8}Ni_{1.3}Mn_{1.3}$ and $FeCr_{0.8}Ni_{1.5}Mn_{1.5}$ alloys. From these results, it is suggested that FeCrNiMn-based high entropy alloys would be developed as high irradiation resistant materials by controlling the stacking fault energy with optimized element concentration.

Keywords: high entropy alloy, stacking fault energy, irradiation, microstructure evolution

*Corresponding author
Naoyuki HASHIMOTO (hasimoto@eng.hokudai.ac.jp)

1. Introduction

In the last decade, the high entropy alloys (HEAs) have been paid attention due to their high strength, ductility, wear resistance, high temperature softening resistance and corrosion resistance compared to conventional metallic material [1-4]. Some of HEAs have been reported as candidate materials for nuclear applications due to their high radiation resistance and corrosion resistance especially at elevated temperatures [5-7]. On the radiation resistance of HEAs, Lu et. al. firstly reported the enhanced swelling resistance at 500 ^{o}C in FCC-type CoCrFeNiMn alloy attributed to the tailored interstitial defect cluster motion from a long-range one-dimensional mode to a short-range three-dimensional mode, which leads to enhanced point defect recombination [8]. Yang et. al. also reported [9] that the irradiated HEAs exhibited a better irradiation tolerance than pure metal at 500 ^{o}C, including slower accumulation of irradiation-induced structural damage and lower void swelling, probably due to both the compositional complexity and alloying elements. Generally, FCC-type materials tend to have a low stacking fault energy (SFE) compared to BCC-type materials, leading to the formation of stacking fault-type defects, such as stacking fault tetrahedron (SFT) and faulted Frank loops (faulted FLs) in matrix, when irradiated in a wide temperature range [10-16]. Those stacking fault-type defects, especially FLs, would be a key of degradation of FCC-type materials under irradiation. W-Y. Chen et. al. investigated the microstructure change in CoCrFeNiMn alloy under irradiation at 300 ^{o}C, found that the size and density evolutions of dislocation loops in the HEA were similar to that in 316H stainless steel [17]. And it is suggested that the loop size and density might be related to the differences in vacancy mobility [17]. On the mobility of point defects in CoCrFeNiMn alloy, Hashimoto et. al. conducted the in-situ electron irradiation experiment and the positron annihilation analysis revealed that Co, Ni, Mn, and Al atoms could affect the vacancy mobility in HEAs but not the interstitial mobility [18]. For the effect of element content on SFE, Mn would play an important

role for the change in the SFE [19]. However, it is noted that these studies on the irradiation resistance were conducted to Co-including FCC-type HEAs.

Concerning about the irradiation response on Co-free HEAs, neutron irradiation experiment revealed that CrFeMnNi HEA showed similar behavior to Fe-Cr-Ni in mechanical strength, phase stability and the annealing of vacancy-type defects, whereas the solute diffusion is slower up to 700 ºC [20]. Parkin et. al. also investigated the irradiation damage in CrFeMnNi-type HEA and found the difference in loop growth kinetics attributed to the difference in Mn-content [21]. This work suggested the detail analysis on the SFE as a useful parameter for determining the irradiation resistance of FCC-type HEAs as well as their strength, ductility, and strain-hardening behavior. In this study, therefore, we focused on Co-free FCC-type FeCrNiMn-based HEAs and investigated the effect of element content on the SFE. Furthermore, in order to clarify the effect of SFE on irradiation damage evolution microstructural changes of those HEAs were investigated by in-situ irradiation experiment.

2. Experimental procedure

The materials used in this study are FCC-type single phase alloys; $FeCr_{0.8}Ni_xMn_y$ (x, y = 1, 1.3, 1.5). The $FeCr_{0.8}Ni_xMn_y$ were prepared by arc-melting method in high-purity argon atmosphere, followed by solution annealing at 1160 °C for 24 hrs. The chemical composition of all the alloys was listed in Table 1. The chemical composition of C, N, and O were analyzed by the combustion infrared absorption method, the inert gas melting-thermal conductivity method, and the inert gas melting-infrared absorption method. For the estimation of SFE, all the alloys were cold-rolled down to 0.25 mm in thick, then punched out for tensile test (SS-J2 type with a gage length of 5 mm). Tensile test was conducted at room temperature, and then, the deformed region was cut and electro-polished to provide for TEM observation. For the in-situ irradiation experiments and

microstructure observation, 3 mmφ TEM disks were punched out from the as-annealed samples and electro-polished. Before the irradiation experiments, macro- and microstructures of the alloys were investigated by using SEM (FE-SEM JEOL JSM6500F) and XRD (Rigaku Fully automatic horizontal multipurpose X-ray diffractometer). In-situ electron irradiation experiment was performed at 400 ºC to 0.2 dpa at the dose rate of 1×10^{-3} dpa/s using the Multi-beam High Voltage Electron Microscope (HVEM operated at 1.25 MeV) at Hokkaido University. The 8MeV Au^{+} ion irradiation was also performed at 500 ºC up to 72 dpa at the dose rate of 6.8×10^{-4} dpa/s for a part of samples by the Takasaki Ion Accelerator for Advanced Radiation Application (TIARA) of the National Institute for Quantum Science and Technology (QST).

3. Results

3.1 Structure and stacking fault energy of $FeCr_{0.8}Ni_xMn_y$

Fig.1 shows the XRD results of $FeCr_{0.8}Ni_xMn_y$ alloys after solution annealing. The profile showed the peaks from (111), (200), (220), (311) and (222) of FCC structure only, indicating that each alloy has the FCC-type single phase structure. In addition, EDS mappings of the alloys showed no concentration gradience or segregation in matrix. Fig. 2 shows the electron backscatter diffraction (EBSD) maps of the $FeCr_{0.8}Ni_xMn_y$ alloys. The average grain sizes of $FeCr_{0.8}NiMn$, $FeCr_{0.8}NiMn_{1.3}$, $FeCr_{0.8}Ni_{1.3}Mn_{1.3}$, and $FeCr_{0.8}Ni_{1.5}Mn_{1.5}$ were 92, 78, 72, and 77 μm, respectively, which would be comparable for the comparison of their mechanical properties. The solution-annealed $FeCr_{0.8}Ni_xMn_y$ alloys included no precipitates but dislocation lines or segments ($<10^{13}$ m^{-2}) in matrix. The 5%-deformed $FeCr_{0.8}Ni_xMn$ alloys included more dislocation lines ($<10^{14}$ m^{-2}) and were used for the estimation of the stacking fault energy. Fig. 3 shows the WBDF images of dissociated dislocations in the deformed $FeCr_{0.8}Ni_xMn_y$ alloys. Those images were taken in the beam condition of $\boldsymbol{B}$ = 111, $\boldsymbol{g}$ = 022, and ($\boldsymbol{g}$/5$\mathbf{g}$). The dissociation width of partial dislocations is

defined as a function of the angle between the dislocation line and the total Burgers vector. The separation distance (d) and the angle (β) between the dislocation and the Burgers vector of full dislocation of these three alloys are measured. The stacking fault energy: γ can be expressed the following equation,

$$\gamma = \frac{G\boldsymbol{b_p}^2}{8\pi d}\left(\frac{2-\nu}{1-\nu}\right)\left(1-\frac{2\nu\cos(2\beta)}{2-\nu}\right)$$

where, G is the shear modulus, $\boldsymbol{b}_p$ is the magnitude of the 1/6$\boldsymbol{a}$<112> partial dislocation Burgers vector ($\boldsymbol{a}$ is the lattice parameter determined by X-ray diffraction) and v is the Poisson's ratio. The Shear modulus and Poisson's ratio of the alloys, measured by resonant ultrasound spectroscopy, were listed in Table 2. Fig. 4 shows the estimated SFE values of $FeCr_{0.8}Ni_xMn_y$ alloys with some previous data points of CoCrFeNiMn type HEAs reported by Liu [22] and Hashimoto [19]. The SFE values of $FeCr_{0.8}Ni_xMn_y$ alloys are higher compared with CoCrFeNiMn type HEAs. Furthermore, the SFE value seemed to be increased with increasing Mn and Ni concentration. From Fig. 4, it seems that Ni concentration dependence on the SFE could be slightly larger than that of Mn.

3.2 Tensile property of $FeCr_{0.8}Ni_xMn_y$

$FeCr_{0.8}Ni_xMn_y$ alloys were tensile-tested at RT at the strain rate of 10^{-4}. Fig. 5 shows the engineering stress - engineering strain curve of all the $FeCr_{0.8}Ni_xMn_y$ alloys. It is noted that the 0.2% proof stress ($\sigma_{0.2}$) and the ultimate tensile strength (UTS) seem to be slightly increasing with increasing Mn and Ni contents., but the total elongation (ε_t) was almost the same among the alloys. And those values were comparable to that of 316H stainless steel [23].

3.3 Microstructural evolution in irradiated $FeCr_{0.8}Ni_xMn_y$

$FeCr_{0.8}Ni_xMn_y$ alloys were electron irradiated at 1×10^{-3} dpa/s to 0.2 dpa at 400 ºC. In this irradiation condition, both self-interstitial atom (SIA) and vacancy can move appreciably [10]. All the alloys remained fully crystalline and retained their original FCC phase with no detectable second phase observed during irradiation experiment. Generally, the electron irradiation introduced point defects in materials, and then, microstructural evolution such as the formation and the growth of SIA cluster (black dot: BD), SIA faulted loops (FL), and cavities would be observed with increasing irradiation dose. Fig. 6 shows the damage microstructure of irradiated $FeCr_{0.8}Ni_xMn_y$ alloys. BDs and FLs were observed in the weak-beam dark-field (WBDF) images. The dark-field (DF) images from relrod showed only FLs on (111) plane. The irradiated $FeCr_{0.8}Ni_{1.5}Mn_{1.5}$ indicated a low number density of (8.7×10^{22} m^{-3}) and the average size (50 nm) of FL compared with the others and even 316SS [24]. A part of FLs could be unfaulted to SIA perfect loops (PL), however, the unfaulting process was not observed in this in-situ irradiation experiment. The critical size for unfaulting of the SIA FLs was not clear [25,26]. Assuming that the critical unfaulting size is depending on the SFE, the SIA FL formation in irradiated $FeCr_{0.8}Ni_xMn_y$ alloys could be controlled by the Ni and Mn concentration. In addition, it is noted that no observable cavities were found in all the $FeCr_{0.8}Ni_xMn_y$ alloys. In order to investigate the formation of cavities and/or vacancy type clusters such as stacking fault tetrahedra (SFT), the Au^+ ion irradiation at 500 ºC up to 72 dpa was performed to $FeCr_{0.8}Ni_{1.3}Mn_{1.3}$ alloy, however, both cavities and SFTs were not found in matrix and even at grain boundaries. Fig.7 summarized the number density and the average size of FL in irradiated $FeCr_{0.8}Ni_xMn_y$. It seems that the number density of FL was decreased with increasing Ni and Mn contents. While, the average size of FL would be almost the same among the $FeCr_{0.8}Ni_xMn_y$ alloys.

4. Discussion

For the estimation of the SFE, G.B. Olson model [27] can be applied. The formula is expressed as below.

$$SFE = 2\rho_A(\Delta G^{FCC\rightarrow HCP} + E^{strain}) + 2\sigma$$

where ρ_A is the atomic density of {111}, $\Delta G^{FCC\rightarrow HCP}$ is the difference of free energy before and after FCC→HCP transformation, E^{strain} is the elastic strain energy of transformation, and μ is the surface energy of FCC/HCP interface. The free energy calculation was performed with using PANDAT-2028 (CALPHAD). Fig. 8 shows that the free energy change of FCC and HCP in $FeCr_{0.8}Ni_xMn$ and $FeCr_{0.8}NiMn_x$ as a function of Ni and Mn contents, respectively. It seems that the increase in Mn and Ni would increase the SFE in this experiment. As shown in Fig. 8, $\Delta G^{FCC\rightarrow HCP}$ is increased with increasing Ni and Mn contents. Therefore, the thermodynamics calculation can support the experimental result of the change in SFE of $FeCr_{0.8}Ni_xMn_y$ alloys. In addition, Ni concentration dependence on the SFE seems to be slightly greater than that of Mn. Lu et al. investigated the effect of Ni and Mn on FeCrNi-based alloys with various Ni contents via quantum–mechanical first-principles calculations [28]. It is found that Mn increases the SFE at room temperature in high-Ni alloys. Furthermore, the first-principles calculations indicated that the intrinsic SFE was predicted to monotonically increase with Mn content in paramagnetic FeMn alloys [29].

The increase in Mn and Ni contents resulted in the increase in SFE, but $\sigma_{0.2}$, UTS, and ε_t were almost the same in $FeCr_{0.8}Ni_xMn_y$ alloys. Generally, the lowering the SFE resulted in the increasing in the work-hardening rate and the deformation twinning formation [30]. In this study, however, less SFE dependence on Tensile property was shown in $FeCr_{0.8}Ni_xMn_y$ alloys.

The electron irradiation experiment resulted in the lowest FL number density in the irradiated $FeCr_{0.8}Ni_{1.5}Mn_{1.5}$, which had the highest SFE among $FeCr_{0.8}Ni_xMn_y$ alloys. G. Bellefon et al.

reported that the SFE value in austenitic stainless steels was empirically evaluated as a function of the chemical composition [31]. The effect of Mn concentration on the SFE appeared to be more significant than the empirical dependence. The formation of SIA FL in FCC-type materials would be affected by the SFE in nature. A previous report indicated that the formation energy of SIA FL is dependent on SFE in nature; however, MD simulation could not indicate any SFE dependence on FL formation [39]. While, on the SIA PL, the critical loop size is obviously dependent on SFE and becomes larger at lower SFE [38]. Concerning about SFE in HEAs, Ni concentration dependence on SFE in CoCrFeNiMn-type HEAs in the range of 14~20 at% Ni [22] has been reported. In the case of the irradiated HEAs, the high Mn concentration in CoCrFeNiMn-type HEAs showed lower number density and smaller loop diameter of FL after Kr^+ ion irradiation at 500 ºC [19]. In this study, Co-free $FeCr_{0.8}Ni_xMn_y$ alloys also showed a similar tendency of the relationship between the FL formation and the SFE.

To correlate the irradiation hardening with microstructure, the Orowan hardening model [32] has been used. The formula is given as follows:

$$\Delta\sigma_y = M\alpha\mu\boldsymbol{b}(ND)^{0.5}$$

where $\Delta\sigma_y$ is the calculated increase in yield strength after irradiation. M is the Taylor factor (3.06 for equiaxed FCC), α is the barrier strength factor (0.4 for FL) [33], μ is the shear modulus (77 GPa for austenitic steels), and $\boldsymbol{b}$ is the Burgers vector of moving dislocation (0.257 nm). N and D are the number density and the size of obstacles, respectively, so that, $\Delta\sigma_y$ can be estimated as a function of $(ND)^{0.5}$. The FL number density (N) and the FL average diameter (D), and $(ND)^{0.5}$ of irradiated $FeCr_{0.8}Ni_xMn_y$ alloys are listed in Table 2. The value of $(ND)^{0.5}$ seems to have the Mn and Ni concentration dependence. The values of $(ND)^{0.5}$ in $FeCr_{0.8}Ni_xMn_y$ alloys were plotted as a function of the estimated SFE (γ) in Fig. 9. From this figure, $(ND)^{0.5}$ can be formulated by following expressions.

$(ND)^{0.5} = (9 \times 10^7) \exp(-0.038\gamma)$

Considering that $FeCr_{0.8}Ni_xMn_y$ showed irradiation resistance compared to CoCrFeNiMn and 316SS, it can be expected that FeCrNiMn-based (Co-free) HEAs could be well-designed by controlling the SFE with optimized element concentration as one of candidate alloys for nuclear applications.

5. Summary

In order to clarify the effect of SFE on irradiation damage evolution in Co-free FCC-type HEAs, the effect of element content on the SFE and microstructure change in $FeCr_{0.8}Ni_xMn_y$ alloys were investigated by in-situ irradiation experiment.

The stacking fault energy of $FeCr_{0.8}Ni_xMn_y$ alloys was increased with increasing both Ni and Mn concentration, $FeCr_{0.8}Ni_{1.5}Mn_{1.5}$ had the highest stacking fault energy, which was much higher value than that of 316SS. The electron irradiation at 400 ºC resulted in the formation of faulted loops, but no observable voids in all the $FeCr_{0.8}Ni_xMn_y$ alloys. The comparison of microstructural evolution revealed less faulted loop formation in $FeCr_{0.8}Ni_{1.3}Mn_{1.3}$ and $FeCr_{0.8}Ni_{1.5}Mn_{1.5}$ alloys, leading to less irradiation hardening compared with a low SFE HEAs and 316SS. From these results, it is suggested that Fe CrNiMn-based HEAs would be one of candidate alloys as high irradiation resistant materials by controlling the stacking fault energy with optimized element concentration.

Acknowledgement

The authors appreciate the special support of Dr. Endo and the great helps of technical stuffs at Nano-Micro Materials Analysis Laboratory of Hokkaido University. This work was supported by JSPS Grant-in-Aid for Scientific Research on Innovative Areas Grant Number JP19H05161.

References

[1] J.-W. Yeh, S.-J. Lin, T.-S. Chin, J.-Y. Gan, S.-K. Chen, T.-T. Shun, C.-H. Tsau, S.- Y. Chou, Formation of simple crystal structures in Cu-Co-Ni-Cr-Al-Fe-Ti-V alloys with multiprincipal metallic elements, Metall. Mater. Trans. A 35 (2004) 2533-2536.

[2] Y.J. Zhou, Y. Zhang, Y.L. Wang, G.L. Chen, Solid solution alloys of $AlCoCrFeNiTi_x$ with excellent room-temperature mechanical properties, Appl. Phys. Lett. 90 (2007) 181904.

[3] C.-Y. Hsu, J.-W. Yeh, S.-K. Chen, T.-T. Shun, Wear resistance and high temperature compression strength of Fcc $CuCoNiCrAl_{0.5}Fe$ alloy with boron addition, Metall. Mater. Trans. A 35 (2004) 1465-1469.

[4] C.-M. Lin, H.-L. Tsai, Equilibrium phase of high-entropy $FeCoNiCrCu_{0.5}$ alloy at elevated temperature, J. Alloys Compd. 489 (2010) 30-35.

[5] D.J.M. King, S.C. Middleburgh, A.G. McGregor, M.B. Cortie, Predicting the formation and stability of single phase high-entropy alloys, Acta Mater. 104 (2016) 172-179.

[6] B. Kombaiah, K. Jin, H. Bei, P.D. Edmondson, Y. Zhang, Phase stability of single phase $Al_{0.12}CrNiFeCo$ high entropy alloy upon irradiation Materials and Design 160 (2018) 1208–1216.

[7] T. Nagase, Philip D. Rack, Joo Hyon Noh, T. Nogami, *In-situ* TEM observation of structural changes in nano-crystalline CoCrCuFeNi multicomponent high-entropy alloy under fast electron irradiation by high voltage electron microscopy, Intermetallics 59 (2015) 32-42.

[8] Chenyang Lu, Liangliang Niu, Nanjun Chen, Ke Jin, Taini Yang, Pengyuan Xiu, Yanwen Zhang, Fei Gao, Hongbin Bei, Shi Shi, Mo-Rigen He, Ian M. Robertson, William J. Weber, Lumin Wang, Nature Communications (2016) 13564.

[9] Tengfei Yang, J. Mater. Res., Vol. 33, No. 19, Oct 14, 2018.

[10] S.J. Zinkle, Radiation-induced Effects on Microstructure, in: R.J.M. Konings (Ed.), Comprehensive Nuclear Materials Vol.1 (2012) 65-98.

[11] G.S. Was, Materials degradation in fission reactors: Lessons learned of relevance to fusion reactor systems, J. Nucl. Mater. 367-370 (2007) 11-20.

[12] M. Li, S.J. Zinkle, Physical and mechanical properties of Copper and Copper alloys, in: R.J.M. Konings (Ed.), Comprehensive Nuclear Materials Vol.4 (2012) 667-690.

[13] T. Muroga, H. Watanabe, Microstructure Response in Copper and Copper Alloys Irradiated with Fission Neutrons with Controlled Temperature Variations, J. ASTM International 1 (9) (2004) 1-10.

[14] B.N. Singh, A. Horsewell, D.S. Gelles, F.A. Garner, Void swelling in copper and copper alloys irradiated with fission neutrons, J. Nucl. Mater. 191-194 (1992) 1172-1176.

[15] F. Mota, I. Palermo, S. Laces, J. Molla, A. Ibarra, Potential irradiation of Cu alloys and tungsten samples in DONES, Nuclear Fusion Vol. 57 (12) (2017) 126056.

[16] R.M. Boothby, in: R.J.M. Konings (Ed.), Comprehensive Nuclear Materials Vol.4 (2012) 123-150.

[17] W-Y. Chen, Xiang Liu, Yiren Chen, Jien-Wei Yeh, Ko-Kai Tseng, Krishnamurti Natesan, J. Nucl. Mater. 510 (2018) 421-430.

[18] N. Hashimoto and Y. Ono, Mobility of point defects in CoCrFeNi-base High Entropy Alloys, Intermetallics 133 (2021) 107182.

[19] N. Hashimoto, T. Fukushi, E. Wada, W-Y. Chen, Effect of stacking fault energy on damage microstructure in ion-irradiated $CoCrFeNiMn_x$ concentrated solid solution alloys, J. Nucl. Mater. 545 (2021) 152642.

[20] Congyi Li, Steven J. Zinkle, Shijun Zhao, Hongbin Bei, Yanwen Zhang, Irradiation responses and defect behavior of single-phase concentrated solid solution alloys, J. Nucl. Mater. 527 (2019) 151838.

[21] C. Parkin, M. Moorehead, M. Elbakhshwan, Jing Hu, Wei-Ying Chen, Meimei Li, Lingfeng He, Kumar Sridharan, Adrien Couet, In situ microstructural evolution in face-centered and body-centered cubic complex concentrated solid-solution alloys under heavy ion irradiation, Acta Materialia 198 (2020) 85-99.

[22] S.F. Liu, Y. Wu, H.T. Wang, J.Y. He, J.B. Liu, C.X. Chen, X.J. Liu, H. Wana, Z.P. Lu, Stacking fault energy of face-centered-cubic high entropy alloys, Intermetallics 93 (2018) 269–273.

[23] Gyeong-Hoi Koo and Ji-Hyun Yoon, Inelastic material models of Type 316H for elevated temperature design of advanced high temperature reactors, Energies 13 (2020) 4548.

[24] J. Gan, E.P. Simonen, S.M. Bruemmer, L. Fournier, B.H. Sencer, G.S. Was, The effect of oversized solute additions on the microstructure of 316SS irradiated with 5 MeV Ni ions or 3.2 MeV protons, J. Nucl. Mater 325 (2004) 94-106.

[25] D. Chen, K. Murakami, K. Dohi, K. Nishida, Z. Li, N. Sekimura, J. Nucl. Mater. 529 (2020) 15192 1-7.

[26] T. Okita, Y. Yang, J. Hirabayashi, M. Itakura, K. Suzuki, Philo. Mag 96 (2016) 1579-1597.

[27] G.B. Olson and M. Cohen: Metall. Trans. A 7 (1976) 1897.

[28] Lu et al. Q-M Hu, B. Johansson, L. Vitos, Acta Materialia 59 (2011) 5728-5734.

[29] Z. Dong, S. Schönecker, D. Chenb, W. Li, S. Lu, L. Vitos, International Journal of Plasticity 119 (2019) 123-139.

[30] S. Huang, W. Li, S. Lu, F. Tian, J. Shen, E. Holmström, L. Vitos, Scripta Mat. 108, 44 (2015) 44-47.

[31] G. Bellefon, J.C. van Duysen, K. Sridharan, J. Nucl. Mater. 492 (2017) 227-230.

[32] E. Orowan: Internal Stresses and Fatigue in Metals, ed. By G.M. Rassweiler and W.L. Grube, Elsevier Sci. Pub. (1959) pp.59-80.

[33] T.S. Byun, N. Hashimoto, K. Farrell, E. Lee, Characteristics of microscopic strain localization in irradiated 316 stainless steels and pure vanadium, J. Nucl. Mater. 349 (3) (2006) 251-264.

Captions of Tables and figures

Table 1 Chemical composition of $FeCr_{0.8}Ni_xMn_y$ alloys (at%).

Table 2 Shear modulus and Poisson's ratio of the alloys, measured by resonant ultrasound spectroscopy.

Table 3 Summary of FL number density (N), FL average diameter (D), and $(ND)^{0.5}$ of irradiated $FeCr_{0.8}Ni_xMn_y$ alloys.

Fig. 1 XRD results of $FeCr_{0.8}Ni_xMn_y$ alloys after solution annealing.

Fig. 2 Electron backscatter diffraction (EBSD) maps of $FeCr_{0.8}Ni_xMn_y$ alloys.

Fig. 3 WBDF images of dissociated dislocations in the deformed $FeCr_{0.8}Ni_xMn_y$ alloys.

Fig. 4 Estimated SFE values of $FeCr_{0.8}Ni_xMn_y$ as a function of Ni and Mn content. The SFE values of $CoCrFeNiMn_x$ also plotted as comparison. [19,22]

Fig. 5 The engineering stress – engineering strain curve of $FeCr_{0.8}Ni_xMn_y$ alloys tested at RT at the strain rate of 10^{-4}.

Fig. 6 Damage microstructure of irradiated $FeCr_{0.8}Ni_xMn_y$ alloys. BDs and FLs were observed in the WBDF images. The DF images from relrod showed only FLs on (111) plane.

Fig. 7 Number density and average size of FL in irradiated $FeCr_{0.8}Ni_xMn_y$. FL number density decreases with increasing Ni and Mn contents. While FL size is independent on element concentration.

Fig. 8 Free energy change of FCC and HCP in $FeCr_{0.8}Ni_xMn$ and $FeCr_{0.8}NiMn_x$ as a function of Ni and Mn contents, respectively.

Fig. 9 The values of $(ND)^{0.5}$ in $FeCr_{0.8}Ni_xMn_y$ alloys as a function of the estimated SFE (γ). $(ND)^{0.5}$ decreases with increasing SFE.

Table 1 Chemical composition of $FeCr_{0.8}Ni_xMn_y$ alloys (at%).

	Fe	Cr	Ni	Mn	C	N	O
$FeCr_{0.8}NiMn$	26.3	21.1	26.3	26.3	0.002	0.007	0.044
$FeCr_{0.8}NiMn_{1.3}$	24.4	19.5	24.4	31.7	0.002	0.005	0.054
$FeCr_{0.8}Ni_{1.3}Mn_{1.3}$	22.7	18.3	29.5	29.5	0.003	0.006	0.035
$FeCr_{0.8}Ni_{1.5}Mn_{1.5}$	20.8	16.6	31.3	31.3	0.002	0.005	0.045

Table 2 Shear modulus and Poisson's ratio of the alloys, measured by resonant ultrasound spectroscopy.

	Shear modulus / GPa	Poisson's ratio
$FeCr_{0.8}NiMn$	62.7	0.30
$FeCr_{0.8}NiMn_{1.3}$	59.5	0.30
$FeCr_{0.8}Ni_{1.3}Mn_{1.3}$	49.9	0.30
$FeCr_{0.8}Ni_{1.5}Mn_{1.5}$	51.1	0.32

Table 3 Summary of FL number density (N), FL average diameter (D), and $(ND)^{0.5}$ of irradiated $FeCr_{0.8}Ni_xMn_y$ alloys.

	Number density (N) /m^{-3}	Average Diameter (D) / nm	$(ND)^{0.5}$ /m^{-1}
$FeCr_{0.8}NiMn$	2.9×10^{21}	48	1.2×10^{7}
$FeCr_{0.8}NiMn_{1.3}$	1.6×10^{21}	30	6.9×10^{6}
$FeCr_{0.8}Ni_{1.3}Mn_{1.3}$	1.1×10^{21}	40	6.6×10^{6}
$FeCr_{0.8}Ni_{1.5}Mn_{1.5}$	8.7×10^{20}	50	6.6×10^{6}

Fig. 1 XRD results of $FeCr_{0.8}Ni_xMn_y$ alloys after solution annealing.

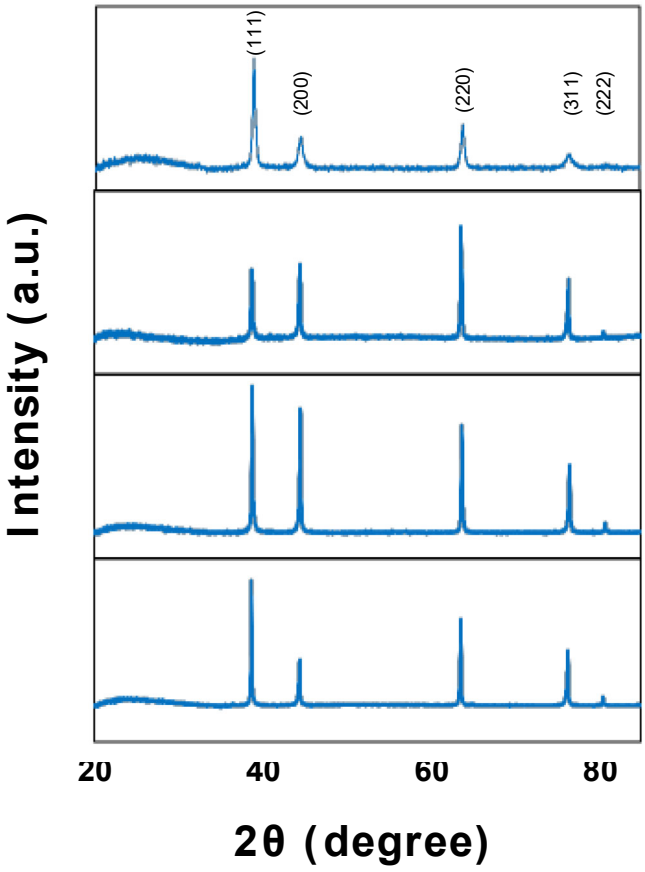

Fig. 2 Electron backscatter diffraction (EBSD) maps of $FeCr_{0.8}Ni_xMn_y$ alloys.

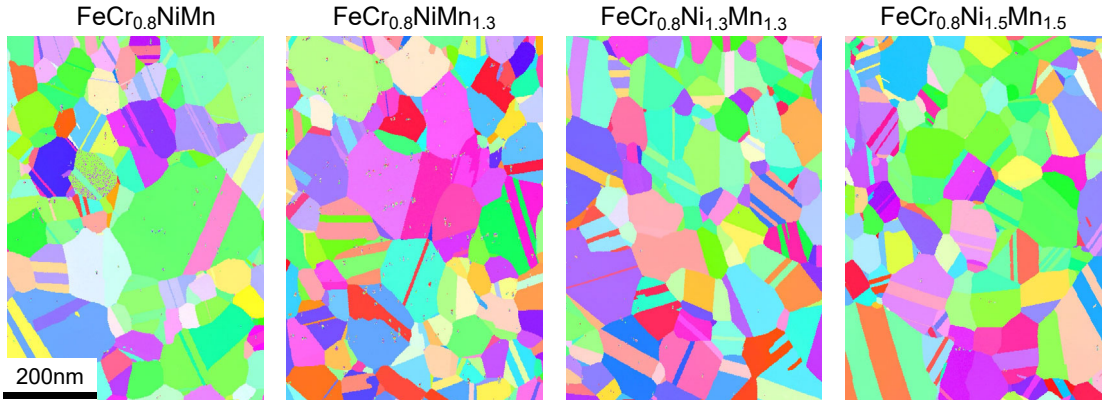

Fig. 3 WBDF images of dissociated dislocations in the deformed $FeCr_{0.8}Ni_xMn_y$ alloys.

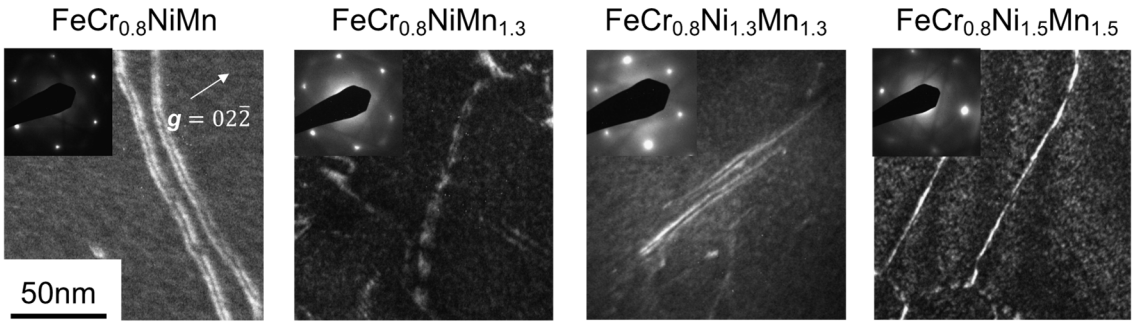

Fig. 4 Estimated SFE values of $FeCr_{0.8}Ni_xMn_y$ as a function of Ni and Mn content. The SFE values of $CoCrFeNiMn_x$ also plotted as comparison. [19,22]

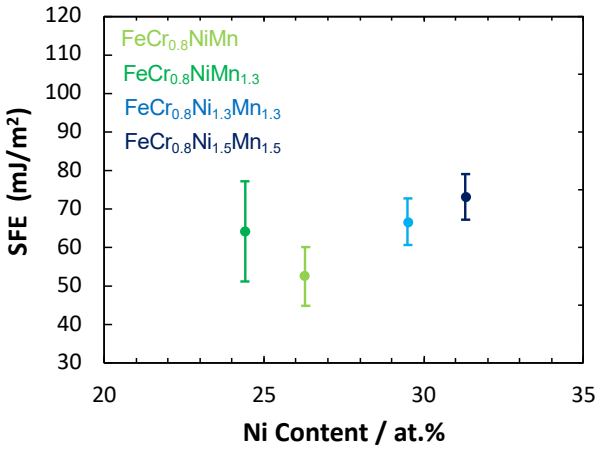

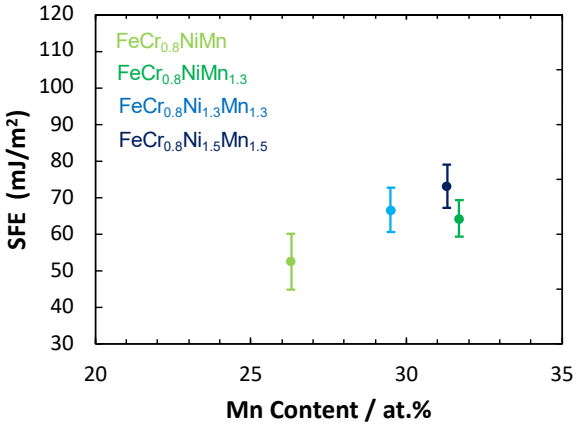

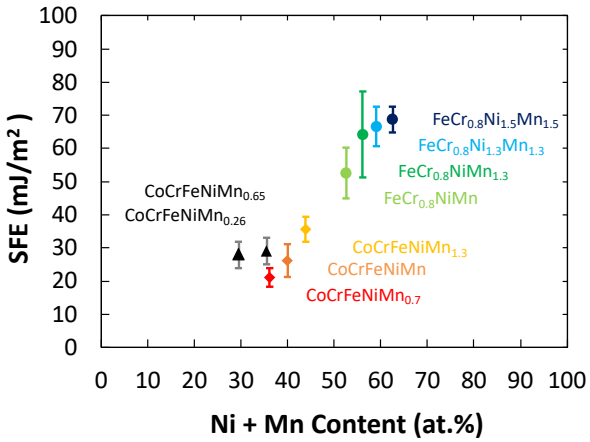

Fig. 5 The engineering stress – engineering strain curve of $FeCr_{0.8}Ni_xMn_y$ alloys tested at RT at the strain rate of 10^{-4}.

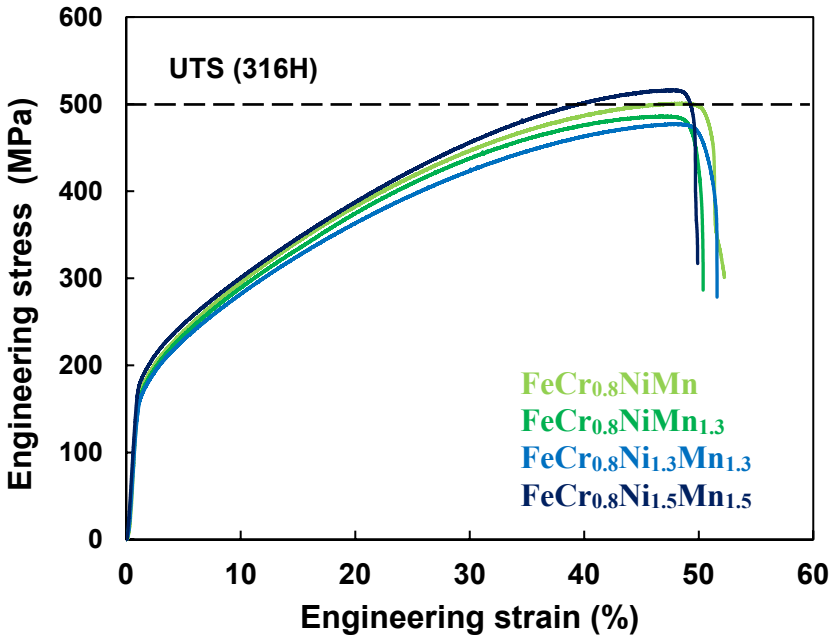

Fig. 6 Damage microstructure of irradiated $FeCr_{0.8}Ni_xMn_y$ alloys. BDs and FLs were observed in the WBDF images. The DF images from relrod showed only FLs on (111) plane.

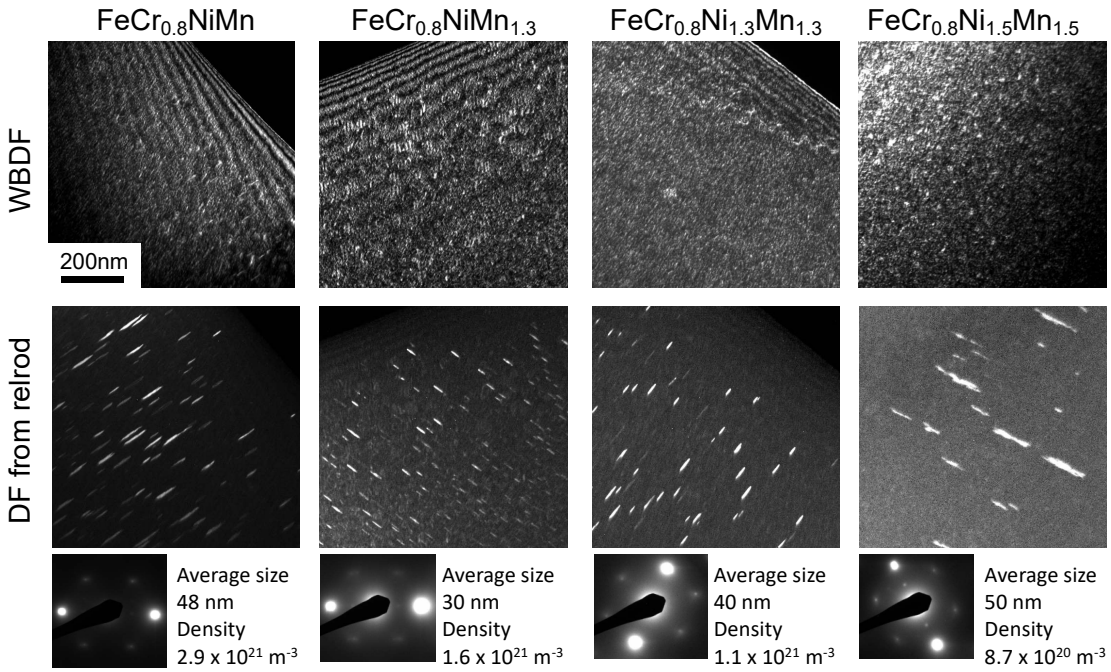

Fig. 7 Number density and average size of FL in irradiated $FeCr_{0.8}Ni_xMn_y$. FL number density decreases with increasing Ni and Mn contents. While FL size is independent on element concentration.

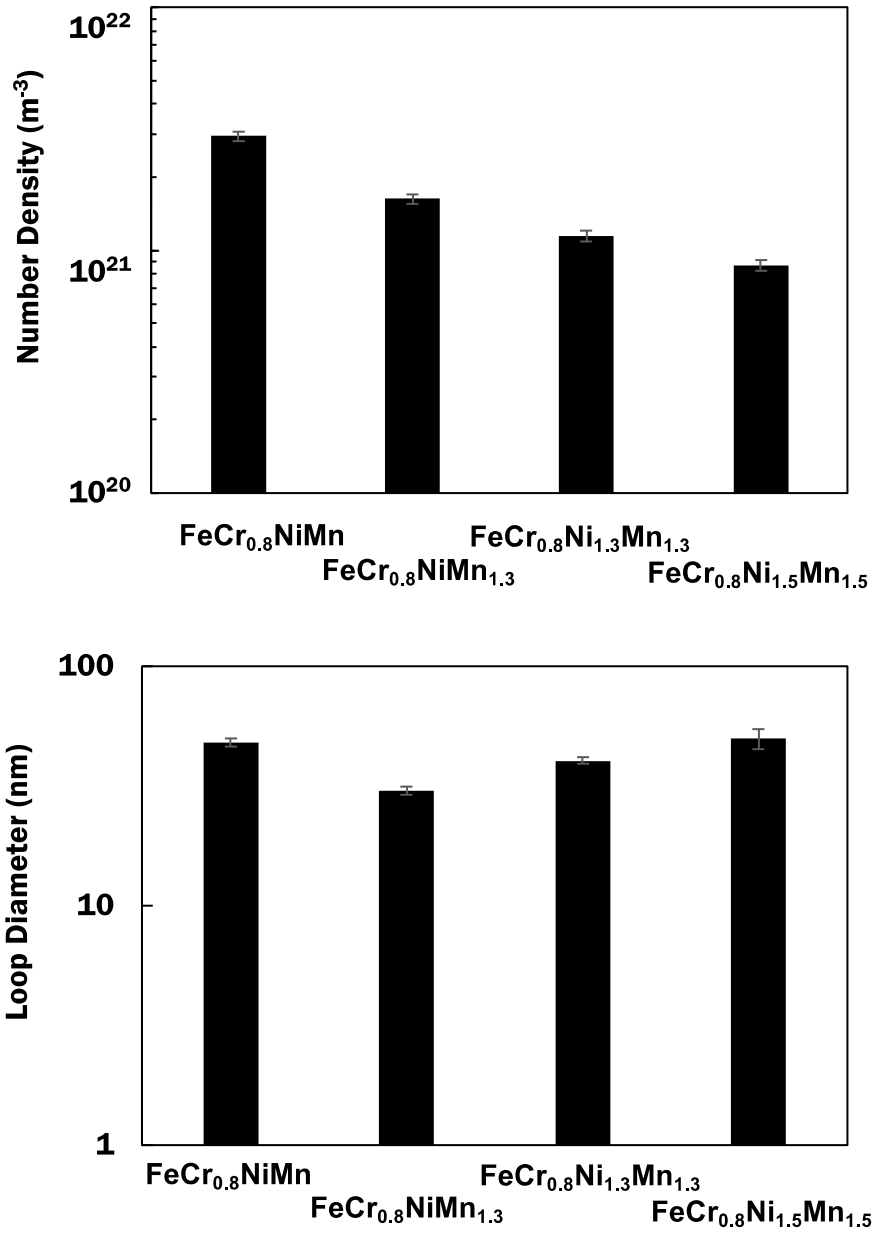

Fig. 8 Free energy change of FCC and HCP in $FeCr_{0.8}Ni_xMn$ and $FeCr_{0.8}NiMn_x$ as a function of Ni and Mn contents, respectively.

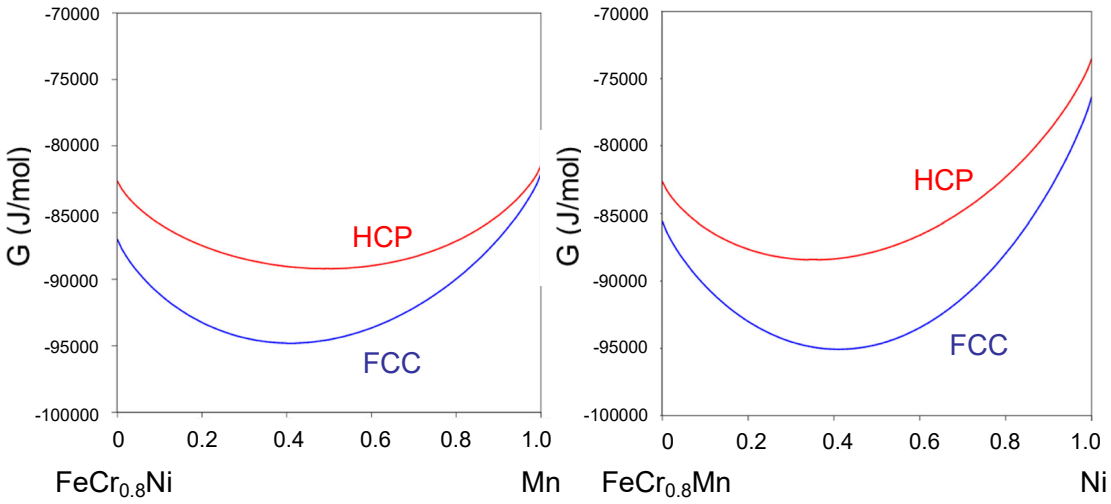

Fig. 9 The values of $(ND)^{0.5}$ in $FeCr_{0.8}Ni_xMn_y$ alloys as a function of the estimated SFE (γ). $(ND)^{0.5}$ decreases with increasing SFE.